Biochimica et Biophysica Acta 1784 (2008) 1050–1058

Contents lists available at ScienceDirect

Biochimica et Biophysica Acta

journal homepage: www.elsevier.com/locate/bbapap

Complex oligomeric structure of a truncated form of DdrA: A protein required for the extreme radiotolerance of *Deinococcus*

Irina Gutsche [a], Andreja Vujičić-Žagar [b], Xavier Siebert [c], Pascale Servant [d], Françoise Vannier [d], Bertrand Castaing [e], Benoit Gallet [f], Thierry Heulin [g], Arjan de Groot [g], Suzanne Sommer [d], Laurence Serre [b,*]

[a] *Unit for Virus Host–Cell Interactions UMR5233 (CNRS/EMBL/Université Joseph Fourier), 6 rue Jules Horowitz, 38042 Grenoble Cedex 09, France*
[b] *Institut de Biologie Structurale UMR5075 (CEA/CNRS/Université Joseph Fourier), Laboratoire des protéines membranaires, 41 rue Jules Horowitz, 38027 Grenoble Cedex 01, France*
[c] *Institut de Biologie Structurale UMR5075 (CEA/CNRS/Université Joseph Fourier), Laboratoire de microscopie électronique et structurale, 41 rue Jules Horowitz, 38027 Grenoble Cedex 01, France*
[d] *Université Paris-Sud, CNRS UMR 8621, CEA LRC42V, Institut de Génétique et Microbiologie, Bâtiment 409, 91405 Orsay Cedex, France*
[e] *Centre de Biophysique Moléculaire UMR4301 CNRS, rue Charles Sadron, 45071 Orléans Cedex 02, France*
[f] *Institut de Biologie Structurale UMR5075 (CEA/CNRS/Université Joseph Fourier), ROBIOMOL / Laboratoire d'ingénierie des macromolécules, 41 rue Jules Horowitz, 38027 Grenoble Cedex 01, France*
[g] *CEA/DSV/IBEB/SBVME Laboratoire d'Ecologie Microbienne de la Rhizosphère et d'Environnements Extrêmes, UMR 6191, Saint-Paul-lez-Durance, F-13108, France*

ARTICLE INFO

Article history:
Received 21 December 2007
Received in revised form 28 February 2008
Accepted 11 March 2008
Available online 3 April 2008

Keywords:
Deinococcus
Radiotolerance
Electron microscopy
DdrA
DNA binding

ABSTRACT

In order to preserve their genome integrity, organisms have developed elaborate tactics for genome protection and repair. The *Deinococcus radiodurans* bacteria famous for their extraordinary tolerance toward high doses of radiations or long period of desiccation, possess some specific genes with unknown function which are related to their survival in such extreme conditions. Among them, *ddrA* is an orphan gene specific of *Deinococcus* genomes. DdrA, the product of this gene was suggested to be a component of the DNA end protection system. Here we provide a three-dimensional reconstruction of the *Deinococcus deserti* $DdrA_{(1-160)}$ by electron microscopy. Although not functional *in vivo*, this truncated protein keeps its DNA binding ability at the wild-type level. $DdrA_{(1-160)}$ has a complex three-dimensional structure based on a heptameric ring that can self-associate to form a larger molecular weight assembly. We suggest that the complex architecture of DdrA plays a role in the substrate specificity and favors an efficient DNA repair.

© 2008 Elsevier B.V. All rights reserved.

1. Introduction

Preserving the genome integrity is an essential process in all organisms, from higher eukaryotes to simple bacteria. For this purpose, living cells have developed strategies to protect, control or repair their genome. Thus, organisms like the non-spore forming bacterium *Deinococcus radiodurans* famous for its extraordinary tolerance toward high doses of ionizing radiations or long period of desiccation, possess molecular machineries particularly well adapted to face severe DNA damage. High irradiation doses introduce multiple breaks inside the DNA molecules generating hundreds of genomic fragments that need to be re-assembled. Remarkably, few hours after an irradiation of 6000 Gy, the genome integrity of *D. radiodurans* is restored. Characterization of several γ-irradiation or desiccation-induced genes showed that, in addition to genes with known function (e.g., *recA* or *polA* [1]), some original genes with unknown function were involved in the extreme radiotolerance of *D. radiodurans* [2,3].

Among these original genes, the DR0423 gene encodes DdrA, a protein evolutionary related to the eukaryotic Rad52 protein [4], an essential component of the recombination process in eukaryotic cells. The biological function of *D. radiodurans* DdrA was investigated and the results indicated that the deletion of the *ddrA* gene increased the *D. radiodurans* sensitivity to ionizing radiation or to mitomycin C and that DdrA contributed to genome restitution [3,5]. Like Rad52, DdrA binds specifically the 3′-extremity of single strand DNA *in vitro* and it is speculated that DdrA could also contribute to the single-stranded annealing [5]. In addition, *in vitro* assays suggested that a putative function of DdrA could be to protect the 3′-ends of single-stranded DNA from nuclease degradation [5]. Apart from *D. radiodurans*, other *Deinococcus* species were isolated and studied for their exceptional radiotolerance [6,7]. Whereas *D. radiodurans ddrA* was described as an orphan gene [3], a homologue was found recently in the *Deinococcus geothermalis* genome [8].

We have recently initiated the characterization of *Deinococcus deserti*, a radiotolerant bacterium isolated from a Sahara sand sample [7]. Here, we present a 3D reconstruction of a truncated form of *D. deserti*, $DdrA_{(1-160)}$, as obtained by negative stain electron microscopy. Our results show that $DdrA_{(1-160)}$ assembles into heptameric rings that can further self-associate into a complex structure.

* Corresponding author. Tel.: +33 438786801; fax: +33 438785494.
E-mail address: laurence.serre@ibs.fr (L. Serre).

1570-9639/$ – see front matter © 2008 Elsevier B.V. All rights reserved.
doi:10.1016/j.bbapap.2008.03.009

2. Materials and methods

2.1. Bacterial strains, cultures, media and transformation

Bacterial strains are listed in Table 1. The *Escherichia coli* DH5α strain was used as the general cloning host, SCS110 strain was used to propagate plasmids prior to transformation of *D. radiodurans*, since this process is sensitive to the methylation status of the transforming DNA [9], and BL21(DE3) strain was used for overexpression and purification of *D. deserti* DdrA. *E. coli* strains were grown in LB medium supplemented with the appropriate antibiotics at the following concentrations: kanamycin 25 μg/ml; spectinomycin, 40 μg/ml. *D. radiodurans* strains used were derivatives of the wild-type strain R1 ATCC13939. *D. radiodurans* was grown in TGY2X broth (1% tryptone, 0.2% glucose, 0.6% yeast extract) at 30 °C with aeration or on TGY1X plates containing 1.5% agar, when necessary supplemented with the appropriate antibiotics at the following final concentrations: chloramphenicol 3 μg/ml; spectinomycin 75 μg/ml. *D. deserti* VCD115 was grown in tenfold-diluted trypticase soy broth (TSB, Bacto-Benton Dickinson). Transformation of *D. radiodurans* with plasmid DNA was performed as previously described [10].

2.2. DNA manipulations

Chromosomal DNA of *D. deserti* was isolated from stationary phase cells in TSB/10 medium. 2 ml cultures were harvested by centrifugation (12 000 rpm at room temperature). Pellets were resuspended in 100 μl of lysis buffer (2% Triton, 1% SDS, 0.1 M NaCl, 0.001 M EDTA) and disrupted with a fastprep desintegrator (Savant; Bio101) using 0.1 g of glass beads (500 μm) in the presence of 100 μl of phenol-chloroform for 120 s. 200 μl of SSC 1× (0.15 M NaCl; 0.015 M tri-sodium citrate) was added. After centrifugation for 3 min at 12 000 rpm, supernatants were treated with one volume of phenol-chloroform-isoamylalcohol (24:1 *v/v*). DNA was precipitated with ethanol and resuspended in 50 μl of TE (0.01 M Tris; 0.001 M EDTA) plus 4 μl of RNase (5 mg/ml). Amplification of genomic DNA by PCR was performed with the Hifi polymerase (ABgene). Oligonucleotides used are listed in Table 2.

2.3. Inverse PCR

The ddrAf1 and ddrAr1 primers designed from *D. radiodurans ddrA* DNA, were used to amplify a *ddrA* DNA fragment from *D. deserti* genomic DNA. After sequencing of the obtained 550 bp PCR fragment, the FV5 and FV6 primers were designed to perform inverse PCR (Table 2). Chromosomal DNA (5 μg) was digested with EaeI. After digestion, DNA was treated with 1 volume of phenol-chloroform and precipitated with 0.3 M sodium acetate in ethanol and resuspended in water. 500 ng DNA was ligated in 200 μl with T4 DNA ligase (Biolabs) overnight at 16 °C. DNA was precipitated and resuspended in 40 μl H_2O. Inverse PCR was carried out on the ligated circular DNA (200 ng), previously denaturated for 15 min at 100°C, using Hifi DNA polymerase (ABgene) in the presence of primers (FV5-FV6). The PCR products contained a major 800 bp fragment that was purified and cloned in the pGEM-TEasy TA cloning vector (Promega), and the nucleotide sequence was determined using universal sequencing primers (T7 promoter, SP6 promoter). FV38/FV49 primers located upstream and downstream of the *ddrA* coding sequence were used to amplify the *ddrA* gene from the genomic DNA of *D. deserti* VCD115 and the sequence was determined.

2.4. Plasmid construction

The plasmid vector designed for *ddrA* complementation, p12721, was obtained by inserting a fragment corresponding to the *D. deserti ddrA* coding sequence (generated by PCR using the FV41/FV44 primers and *D. deserti* genomic DNA as template) between NdeI/XhoI sites of p11559 [11]. The plasmid vector designed for truncated-*ddrA* complementation, p12741, was obtained by inserting a fragment corresponding to the *D. deserti* truncated *ddrA* gene (generated by PCR using the FV41/FV68 primers and *D. deserti* genomic DNA as template) between NdeI/XhoI sites of p11559 [11].

DdrA was overproduced in *E. coli* using p12713. This plasmid was constructed by cloning a NdeI/BamHI DNA fragment, corresponding to the *D. deserti ddrA* sequence (generated by PCR with the FV41/FV43 primers and *D. deserti* genomic DNA as template) between the NdeI/BamHI sites of pET-TEV [12]. All constructions were verified by DNA sequencing.

Table 1
Bacterial strains and genotypes

Strains	Genotype or other relevant characteristics	Source or reference
E. coli		
DH5α	*supE44 ΔlacU(ϕ80lacZΔM15) hsdR17 recA1 endA1 gyrA96 thi-1 relA1*	Laboratory stock
SCS110	*endA dam dcm supE44 Δ(lac-proAB) (F'traD36 proAB lacI^{q}ZΔM15)*	Laboratory stock
BL21 (DE3)	F' *ompT hsdS$_B$ gal dcm* (λDE3)	Laboratory stock
D. radiodurans		
R1	ATCC13939	[31]
GY10973	as R1 but *amyE* Ω(P*tufA*::*lacI kan*)	[32]
GY12362	as GY10973 but Δ*ddrA*::*cat*	[22]
GY11921	R1/p11559	This work
GY12803	*amyE* Ω(P*tufA*::*lacI kan*) Δ*ddrA*::*cat*/p11559	This work
GY12806	*amyE* Ω(P*tufA*::*lacI kan*) Δ*ddrA*::*cat*/p12721 (*D. deserti ddrA*$^+$)	This work
GY12826	*amyE* Ω(P*tufA*::*lacI kan*) Δ*ddrA*::*cat*/p12741 (*D. deserti ddrA* $^+_{truncated}$)	This work
D. deserti		
VCD115	Isolated from Sahara sand	[7]

Table 2
Overview of the oligonucleotides used in this study

Primer	Primer sequence (5′ to 3′)	Use
Amplification of ddrA fragment		
ddrAf1	AAGCTGAGCGATGTCCAGAA	Amplification of *ddrA* fragment
ddrAr1	GCGGCCTTGAGGTGCTTGTA	Amplification of *ddrA* fragment (c)
Inverse PCR		
FV 5	ACCTGGTGCAGGCCATGGAT	Amplification of *ddrA*
FV 6	CAATGTGAGCCAGCATCAAC	Amplification of *ddrA* (c)
Sequencing		
FV 38	AGAGGAATTACGCCTTGACC	Amplification of *ddrA*, on upstream region
FV 49	CGGCCATAGCCAGCTGCAAT	Amplification of *ddrA*, on downstream region (c)
Cloning of ddrA		
FV 41	TTAA**CATATG**AAGCTGAGCGATGTAC	Amplification of *ddrA* or truncated *ddrA* to clone in p11559 or pET-TEV
FV 43	TAA**GGATCC**TCATGCGGCGCGGCCCTG	Amplification of *ddrA* to clone in pET-TEV (c)
FV 44	TAA**CTCGAG**TCATGCGGCGCGGCCCTGG	Amplification of *ddrA* to clone in p11559 (c)
FV 68	TAA**CTCGAG**TTACTGCACCAGGTGAGCGC	Amplification of truncated *ddrA* to clone in p11559 (c)
Mutagenesis of ddrA		
CTCACCTGGTGCAGTAAATGGATCAGCTGCG		
CGCAGCTGATCCATTTACTGCACCAGGTGAG		
DNA binding assay		
*Oligo 1	GGTCTTTCAAATTGTATAAGGAAGAAACTAATGCTAGCGACGGTCAGAGGC	
Oligo 2	GCCTCTGACCGTCGCTAGCATTAGTTT CTTCCTTATACAATTTGAAAGACC	
*Oligo 3	GAAACTAATGCTAGCGACGGTCAGAGGCGGTCTTTCAAATTGTATAAGGAA	
Oligo 4	GCCTCTGACCGTCGCTAGCATTAGTTTC	

Tags with restriction site are in bold. (c) Sequence is on the complementary strand. Among the single-stranded oligonucleotides designed for the DNA binding assay, complementary sequences are underlined and radio-labelled oligonucleotides are indicated by an asterisk.

2.5. Expression and purification of the full-length DdrA protein

10 ml of an overnight culture of *E. coli* BL21(DE3) derivatives containing the p12713 plasmid were used to inoculate 1 l of LB medium supplemented by 25 μg/ml kanamycin. Overexpression of the protein was induced by the addition of 0.1 mM IPTG at A_{600}=0.5. After 2 h, cells were collected, then resuspended in 1 M NaCl, 0.05 M Tris–HCl pH 8.0 and a cocktail of anti-proteases (Roche), and broken by the French press method. The supernatant resulting of a 15 000 rpm centrifugation was mixed with Ni-NTA beads (Qiagen) at 4°C. After an extensive washing step, the protein was eluted by 0.15 M Imidazole, 1 M NaCl, 0.05 M Tris–HCl pH 8.0. The purest fractions were pooled and concentrated with a large cutoff (100 kDa) centricon. Mass spectroscopy was performed on these samples (Applied Biosystems Voyager system 125). For all the experiments carried out in this study (DNA binding and electron microcopy), a final step of gel filtration chromatography was added to the purification protocol (performed on a Superdex 200 HiLoad 16/60 column (GE) pre-equilibrated in (0.15 M NaCl, 0.02 M Tris–HCl pH 7.5). One single peak was observed. SDS-PAGE (12%) gel analysis of this peak indicated two major bands at 24 and 20 kDa (Fig. 1).

The secondary structures and linker region predictions of *D. deserti* DdrA were performed with the Jpred [13] and DPL [14] programs. Isoelectric points were determined by ProtParam [15].

2.6. Expression and purification of the truncated form of DdrA

An additional stop codon was introduced in the wild type *ddrA* gene on plasmid p12713 using the mutagenesis kit (Stratagene) and the oligonucleotides listed in

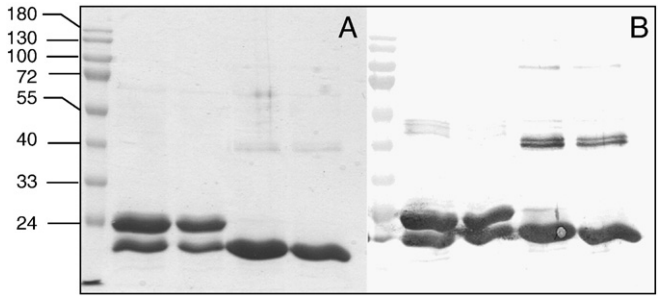

Fig. 1. SDS-PAGE analysis of the protein samples after size exclusion chromatography. These samples were purified according to the protocol described in the Materials and methods section. The different gel lanes correspond to: Molecular weight markers (lanes 1, 6), 40 μg of full-length DdrA (lanes 2, 7): 20 μg of full-length DdrA (lanes 3, 8); 40 μg of $DdrA_{(1-160)}$ (lanes 4, 9) 20 μg of $DdrA_{(1-160)}$ (lanes 5, 10). A) Proteins are revealed by Coomassie Blue staining. B) Proteins are revealed by His-tag western blotting.

Table 2. The purification of $DdrA_{(1-160)}$ was carried out using the same protocol described above for the full-length protein. SDS-PAGE gel analysis of the elution peak obtained after the gel filtration indicated one single major band at 20 kDa and several minor bands corresponding to higher molecular weight species of $DdrA_{(1-160)}$ (Fig. 1).

2.7. Negative stain electron microscopy

Different fractions of the peak eluted from the gel filtration column were collected and observed separately by negative stain electron microscopy. The sample was applied to the clean side of a thin carbon film on carbon–mica interface. The carbon film with the absorbed sample was floated on a drop of NanoW solution (Nanoprobes Inc.). A 400-mesh copper grid was put on top of the floating carbon film and the whole was turned upside down and used to catch a second layer of carbon film floating on another drop of NanoW. Prepared this way, the sample was entirely and uniformly stained and trapped between two thin layers of carbon. The grids were observed under low-dose conditions with a JEOL 1200 EX II transmission electron microscope with a tungsten filament at 100 kV. Visual inspection indicated that all the fractions contained a small ring-shaped species, together with some larger species. The most distal fraction seemed the most homogeneous and we focused our analysis of this particular fraction. Images were recorded on Kodak SO-163 films at a nominal magnification of 40 000× and the negatives were digitised on a Zeiss SCAI scanner at a pixel size of 7 μm, corresponding to 1.75 Å/pixel at the specimen level.

2.8. Image analysis

Image processing was carried out on a Linux workstation using the IMAGIC [16] and EMAN [17] software packages. Using EMAN image processing software, the images were binned to 3.5 Å/pixel at the specimen level. 15166 subframes containing individual $DdrA_{(1-160)}$ particles were selected interactively from micrographs at different *defoci* to better fill the zeroes of the contrast transfer function. A phase-reversal correction was done for each set of subframes corresponding to a particular defocus independently, before combining the sets and low path filtering all the images at 15 Å resolution in real space. Subsequent data processing was performed with the IMAGIC package [16]. The data set was translationally but not rotationally aligned relative to the rotationally averaged total sum of the individual images. The aligned data set was subjected to multivariate statistical analysis (MSA) and classification, which allowed to separate the big species from the small ring-shaped species and demonstrated clearly the 3-fold rotational symmetry of the large $DdrA_{(1-160)}$ oligomer. The characteristic class averages of the large oligomer were then used as a set of references for multi-reference alignment (MRA) followed by MSA and classification. After several rounds, six best views were selected to generate an initial model of the $DdrA_{(1-160)}$ oligomer by angular reconstitution with an imposed C3 symmetry. This first 3D model was used to create an anchor-set and refine the Euler angle determination. An intermediate 3D model obtained after several iterations of 3D-reconstruction and anchor-set refinement was projected into the asymmetric triangle for the C3 symmetry to provide a set of 3D-centered references for new rounds of MRA and angular reconstitution. Refinement of the 3D model was done in parallel in EMAN and IMAGIC and led to indistinguishable reconstructions. The resolution of the reconstruction was estimated via Fourier shell correlation to be around 23 Å according to the 0.5 threshold. A fit of the crystal structure of the homologous-pairing domain of human Rad52 protein (extracted from the PDB file 1KN0) into the electron microscopy reconstruction was done with the UROX software [18] (http://mem.ibs.fr/UROX). Only the N-terminal domain residues ranged from 25 to 178 of Rad52 were considered for the fitting. The last C-terminal residues from 179 to 209 were excluded because they include a loop region in the crystal structure.

The buried accessible surface was estimated by AREAIMOL from the CCP4 package [19].

2.9. γ-irradiation of D. radiodurans bacteria

Bacteria containing p11559 derivatives were grown in TGY2X media supplemented with spectinomycin and IPTG 10 mM. Late exponential phase cultures (A_{650} = 1.5) were concentrated ten times in TGY2X and irradiated on ice with a ^{137}Cs irradiation system (Institut Curie-Orsay, France) at a dose rate of 56.6 Gy/min. Following irradiation, diluted samples were plated on TGY plates supplemented with 1 mM IPTG and incubated 3–4 days at 30 °C before the colonies were counted.

2.10. Oligonucleotides and DNA binding assay

The different oligonucleotides used for this assay are listed in Table 2 and described in Fig. 2. Their nucleotide sequences were checked by a RNA/DNA fold program (Vienna RNA package [20]) to remove all possible secondary structures of the single strand DNA. Single-stranded oligonucleotides (oligo 1 to 4) used for electromobility shift assay (EMSA) were purchased from Eurogentec and purified by Urea-PAGE in sequencing gel. Oligo 1 and oligo 3 were then 5′-[^{32}P]-labeled before annealing with their cold complementary strands to generate different DNA duplexes schematized in Fig. 2. The DNA binding activity of both full-length and truncated $DdrA_{(1-160)}$ was tested by EMSA which was performed as previously described [5]. DNA binding experiments were performed in a 10 μl reaction mixtures containing reaction buffer (0.05 M Tris–HCl, pH 7.4, 0.1 M NaCl, 0.5 mM EDTA, 1 mM DTT, 10% (*v*/*v*) glycerol), 1.25 nM of ^{32}P-labeled DNA duplex or 5 nM ^{32}P-labeled single-stranded DNA (oligo 1) and 40 nM of protein. Reaction mixtures were incubated at 30 °C for 20 min. Samples were loaded on a 10% native polyacrylamide gel and electrophoresis was performed at room temperature in 1× TBE buffer (0.1 M Tris–borate, pH 8.0, 2 mM EDTA) with a 1 h pre-run at 400 V followed by a 3 h run at 500 V.

3. Results

DdrA is an orphan gene specific of *Deinococcus* genomes. It has been clearly identified as related to the extraordinary radiotolerance of these bacteria [3,5]. We have amplified a 550 bp DNA fragment, using primers designed for *D. radiodurans ddrA* gene and *D. deserti* genomic DNA as template. After sequencing of the amplified fragment, an inverse PCR was performed on *D. deserti* genomic DNA to obtain the 5′ and 3′ ends of the *D. deserti ddrA* gene and the 800 bp major DNA fragment obtained was cloned in pGEM-TEasy and sequenced. Then, primers were designed to amplify from *D. deserti* genomic DNA a 694 bp fragment containing the *ddrA* coding sequence, 49 bp upstream the initiation ATG codon and 39 bp downstream of the TGA stop codon. Fig. 3 shows that DdrA is a very conserved protein in *Deinococci*. The functionality and the involvement in DNA repair of the *D. deserti* DdrA protein was tested in a *D. radiodurans* host deprived of its own DdrA protein. *D. deserti ddrA* gene was cloned on an expression vector and expressed from a P_{Spac} promoter in Δ*ddrA D. radiodurans* bacteria. *D. radiodurans* was chosen rather than *D. deserti* because a *ddrA* mutant strain and genetic tools were available for the former. Whereas the *D. radiodurans* cells deficient in DdrA were radiosensitive, the expression of the wild type *D. deserti* DdrA protein in the *D. radiodurans* Δ*ddrA* bacteria was sufficient to fully restore radio-resistance (Fig. 4). As *D. deserti* DdrA exhibits 80% sequence identities with its *D. radiodurans* homologue (Fig. 3), these results strongly suggest a high conservation of the DNA repair mechanisms involving DdrA activity and probably a high conservation of all the factors interacting with DdrA in these processes.

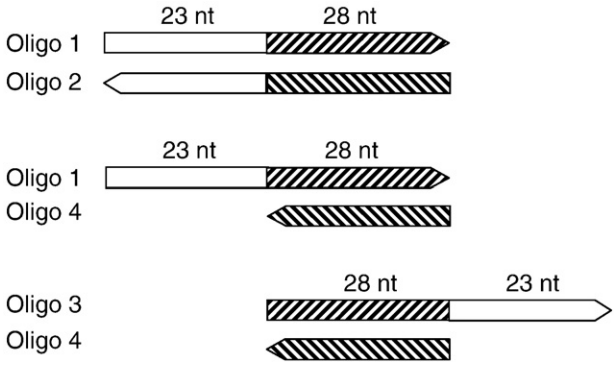

Fig. 2. Different DNA duplexes formed from the four oligonucleotides and used in this study in the DNA binding assay. The complementary regions are colored in dark. The detailed oligonucleotide sequence is described in Table 2.

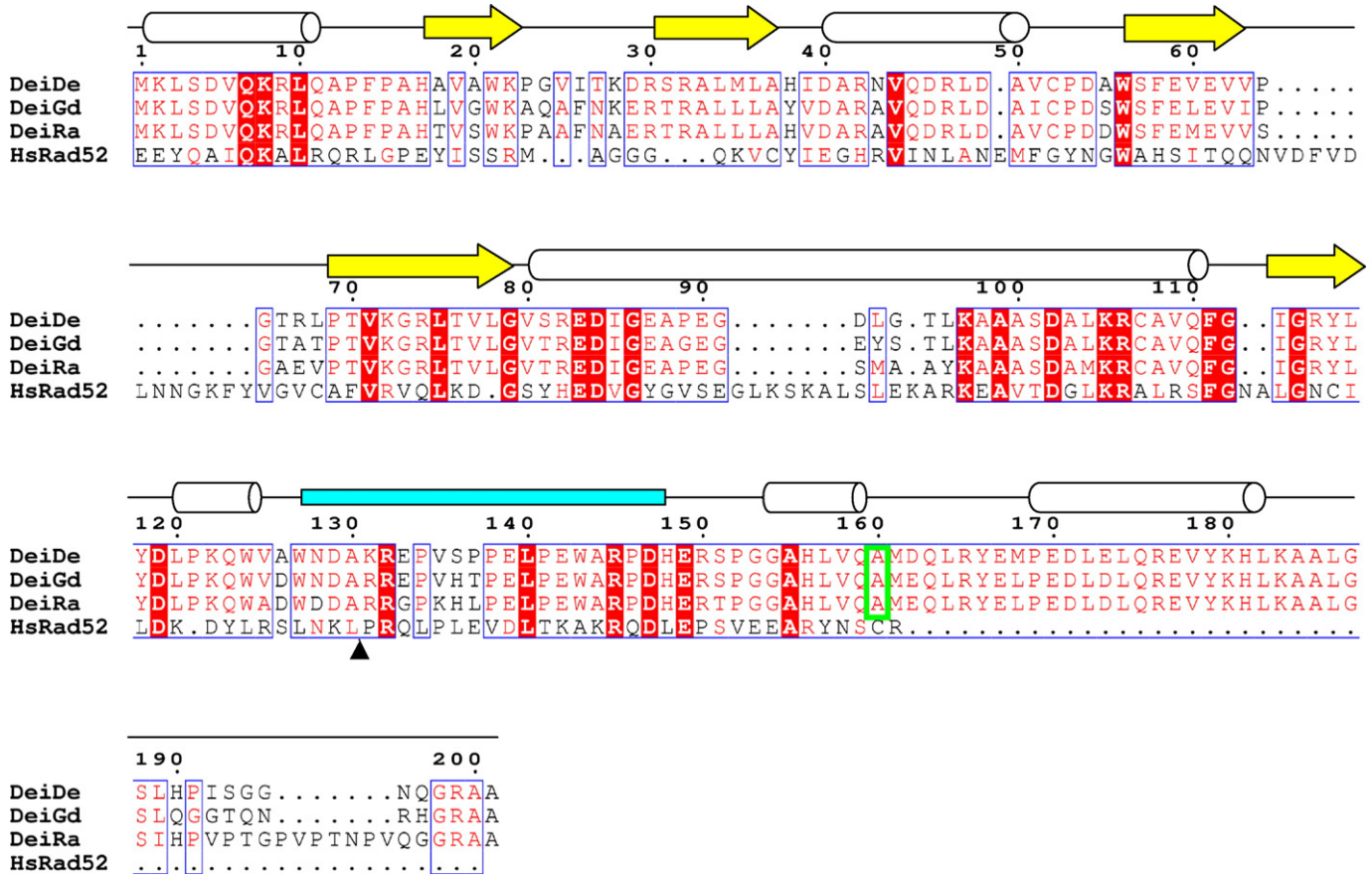

Fig. 3. Primary sequence alignment of DdrA from *D. deserti* (DeiDe), *D. geothermalis* (DeiGd), *D. radiodurans* (DeiRa) and the N-terminal domain of human Rad52 (HsRad52) represented by EsPript [30]. The alignment of human Rad52 and *D. radiodurans* DdrA was deduced from [4]. Secondary structures and domain linker were predicted with the Jpred and the DPL programs [13,14]. Predicted α-helices and β-strands are represented by white cylinders and yellows arrows, respectively. The possible linker region is colored in cyan. The last C-terminal residue of $DdrA_{(1-160)}$ is framed in green. The C-terminus of the Rad52 model used for the fitting in the EM reconstruction is indicated by a black arrow.

3.1. The N-terminal domain of D. deserti DdrA pilots the oligomerization process

We overexpressed the *D. deserti* gene in *Escherichia coli*. During the last purification step of the recombinant DdrA, we observed that the purified protein was eluted in the exclusion volume of the gel filtration column suggesting a high molecular weight object. The analysis of the elution peak on a SDS-PAGE (12%) indicated the presence of several bands: two major bands at approximately 24 kDa and 20 kDa and several minor bands corresponding to DdrA oligomers (Fig. 1A). The 24 kDa band matched the molecular weight predicted for the full-length 6×His-tagged protein. Western blot analysis based on an anti-6×His antibody coupled to the horse radish peroxidase, demonstrated that each of those bands corresponded to different DdrA forms that exhibit the same N-terminal sequence (Fig. 1B). In addition, the mass spectrometry analysis of the wild type protein indicated the presence of three different polypeptides in our purified protein sample: 24.5 kDa, 19.7 kDa and 4.8 kDa. The presence of the 4.8 kDa fragment that should have been eliminated during the gel filtration chromatography, indicates that after cleavage, this peptide still interacts with the rest of the protein.

These different controls allowed us to predict the location of a cleavage sensitive sequence near the A160 residue (Fig. 3). Interestingly, a similar cleavage pattern was observed, however to a lesser extent, for the *D. radiodurans* homologue [5] suggesting that this might be a structural feature common to all the *Deinococcus* DdrAs with a potential biological sense (for example, in the degradation or regulation pathway of the protein).

Attempts to avoid this cleavage were unsuccessfull. Therefore, to obtain a homogenous protein sample more suitable for its electron microscopy study, an additional stop codon was introduced inside the wild type gene by site-directed mutagenesis, yielding a truncated form named $DdrA_{(1-160)}$. As observed for the full-length protein sample, this shorter form kept its properties of oligomerization. Preliminary electron microscopy observations of different $DdrA_{(1-160)}$ samples still suggested some heterogeneity, even though the protein eluted from the gel filtration column appeared as a single nearly symmetrical peak. Different fractions of the peak were collected separately and we observed that the distal fractions looked the most homogenous under the electron microscope (Fig. 5). These results show that the removal of the last C-terminal residues does not prevent the subunit assembly and the oligomerization of DdrA requires only the N-terminal part of the protein (residue 1 to 160).

3.2. The truncated form of D. deserti DdrA keeps its DNA binding properties but is not functional in vivo

The secondary structures prediction pointed out that the *D. deserti* DdrA protein would be made up of two domains: one major α/β domain composed of residues 1 to 125 and one small helical domain composed of residues 151 to 202 that includes the cleavage site we mentioned previously. Both domains would be connected by a proline-rich polypeptide linker (Fig. 3). The calculation of the theoretical isoelectric point on each of these domain highlighted that the charged residue distribution is not homogenous along the primary structure: the largest domain of DdrA is much more basic (p*I*=9.0)

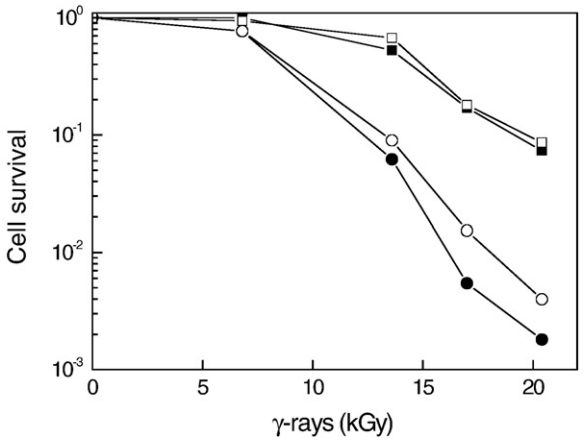

Fig. 4. Survival curves for *D. radiodurans* mutant Δ*ddrA* complemented by *D. deserti ddrA* gene following exposure to γ-irradiation. Symbols: wild type (closed squares); Δ*ddrA* (closed circles); Δ*ddrA*/ p12721 (*D. deserti ddrA*$^{+}$) (open squares); Δ*ddrA*/ p12741 (*D. deserti ddrA*$^{+}_{(1-160)}$) (open circles). Bacterial strains were exposed to γ-irradiation and cell survival was measured as described in Materials and methods. Each value is the average of three independent experiments with standard deviations that did not exceed 10% of the mean values.

than the C-terminal domain including the linker region (p*I*=5.7). This observation strongly suggests that the larger domain of DdrA could be crucial for the DNA binding.

We tested the DNA binding ability of our samples of purified *D. deserti* DdrA (one containing a mixture of the 24.5 kDa, 19.7 kDa and 4.8 kDa polypeptides, and one sample consisting in pure truncated DdrA$_{(1-160)}$) by EMSA and we compared these results with the previous work carried out with the purified *D. radiodurans* DdrA [5]. In these conditions, Fig. 6 shows that both samples behave like the *wt D. radiodurans* DdrA [5], *i.e.*, both species of purified *D. deserti* DdrA bind efficiently to single-stranded DNA, they do not interact with double-stranded DNA fragments exhibiting blunt ends and show a strong binding preference for 3′-cohesive ends rather than 5′-cohesive extremities. This DNA binding assay demonstrates clearly that the removal of the last C-terminal residues does not affect the DNA binding property of the multimeric protein. The N-terminal domain is therefore essential for the interaction with the DNA, which is in agreement with the strong basic character of this domain as predicted by the isoelectric point calculation.

We then tested if the truncated DdrA protein was functional and able to restore the radiotolerance phenotype of *D. radiodurans*. Fig. 4 shows that expression of the *D. deserti* truncated DdrA$_{(1-160)}$ is not sufficient to compensate the absence of the wild type *D. radiodurans* DdrA protein.

3.3. The three-dimensional structure of *D. deserti* DdrA$_{(1-160)}$ is based on a heptameric unit

The oligomerization property of the purified DdrA$_{(1-160)}$ was clearly visualized by negative stain electron microscopy (Fig. 5). Two

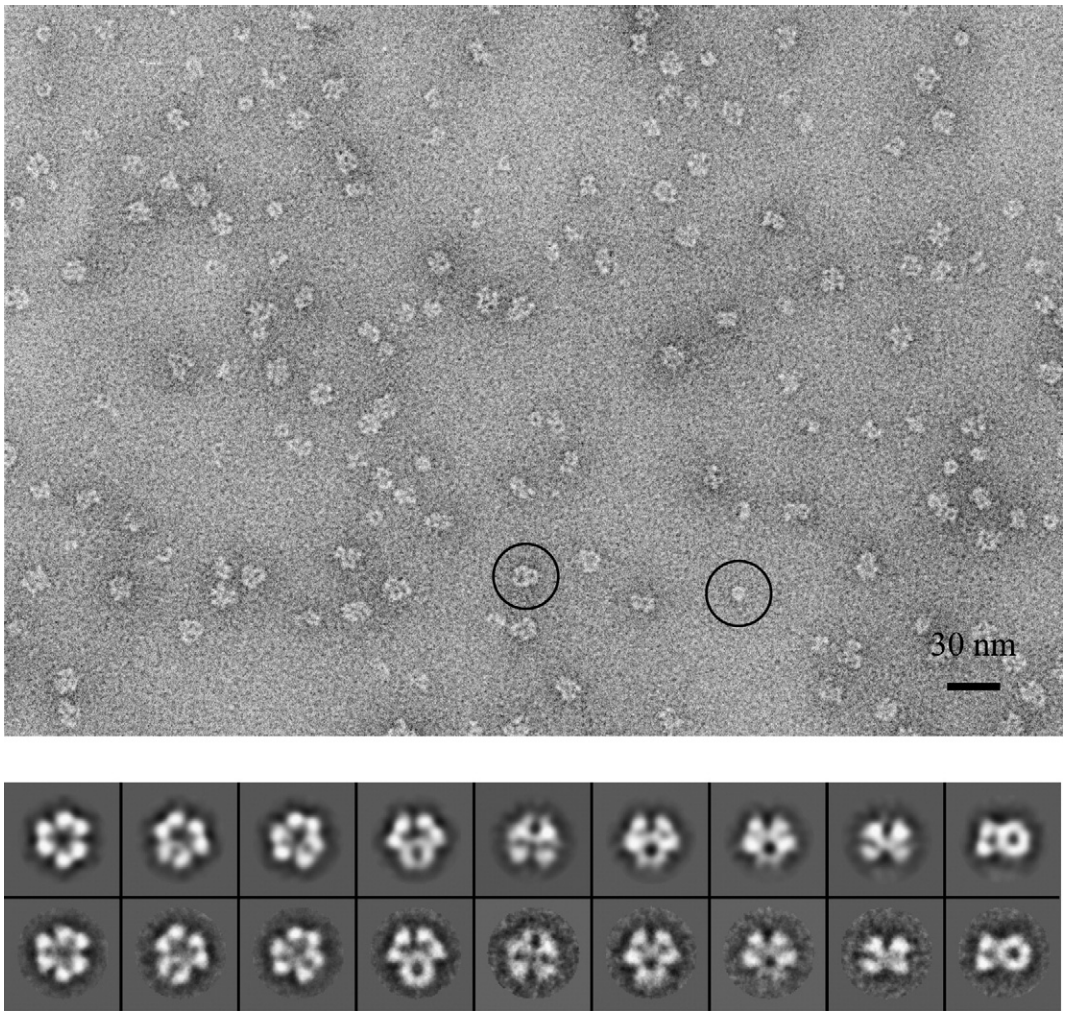

Fig. 5. Negative stain electron microscopy of *D. deserti* DdrA$_{(1-160)}$. A) A field of a micrograph with two types of assemblies highlighted. B) Projections of the three-dimensional reconstruction of the large complex into nine different directions (top) and corresponding class averages (bottom).

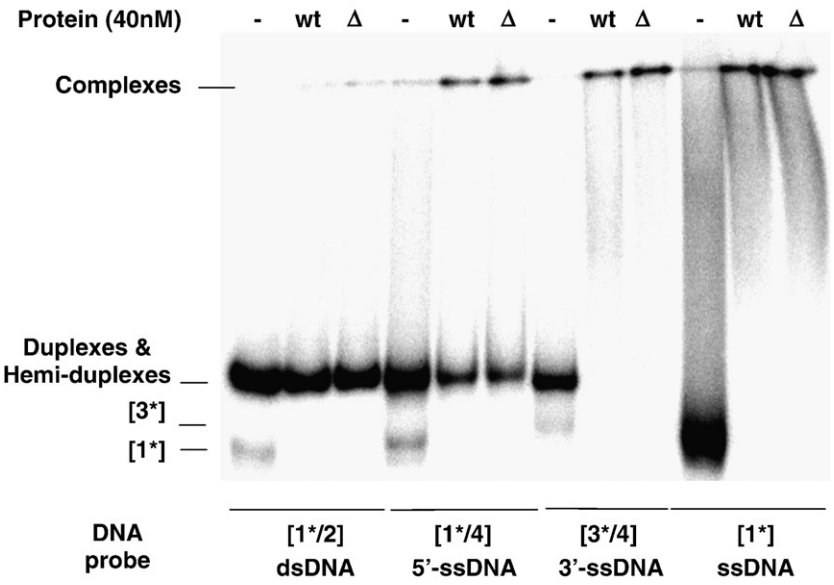

Fig. 6. DNA binding analyzed by EMSA. wt and Δ correspond to the protein samples we analyzed by mass spectroscopy that contains a mixture of polypeptides and the purified $DdrA_{(1-160)}$, respectively. [DNA probe] final concentration is 1.25 nM.

types of assemblies could be detected right away from these images: smaller ring-shaped species of 7.5 nm (Fig. 5, right circle) in diameter and larger ones about 13.5 nm in size (Fig. 5, left circle). The latter ones were randomly oriented on the grid and some of their projections clearly indicated that the largest objects were composed of rings of the same dimensions as the small particles. From these observations, it was inferred that the small ring-shaped species constituted the building blocks of the large $DdrA_{(1-160)}$ complex.

We attempt to determine the symmetry of the small species by multivariate statistical analysis using the IMAGIC software package [16]. However only 7% of the selected subframes represented isolated rings and the majority of those corresponded to broken, distorted or slightly tilted particles. Even a selection of small particles from 20 additional micrographs could not provide enough ring projections along the rotational symmetry axis for a clear symmetry determination. As for the large $DdrA_{(1-160)}$ complex, multivariate statistical analysis unambiguously demonstrated its 3-fold symmetry. Inspection of characteristic views obtained after classification suggested that the large complex was assembled from three $DdrA_{(1-160)}$ rings (Fig. 5). A three-dimensional reconstruction of the 3-ring particle was performed by angular reconstitution. The large complex resembles a basket made of three flower-shaped rings and the top of the basket is slightly more open than the bottom. The angle between the local rotational axis of the ring building blocks and the 3-fold axis of the whole complex is about 120°. Each ring seemed to be composed of seven $DdrA_{(1-160)}$ subunits. To further improve the resolution of the reconstruction, one individual ring was cut out of the 3-ring $DdrA_{(1-160)}$ particle and symmetrized 5, 6, 7, 8 and 9-fold. Only the 7-fold symmetrized ring manifested clearly reinforced structural features. In addition, an artificial featureless doughnut of the same dimensions as the $DdrA_{(1-160)}$ ring was created. A set of new 3D models was then built out of each type of these artificially produced rings re-assembled back into a 3-ring structure. After several cycles of projection matching with only the C3-symmetry imposed, all the models converged to the same final structure of the 3-ring $DdrA_{(1-160)}$ (Fig. 7). The resolution of the final reconstruction is about 23 Å. To check carefully the symmetry of each individual ring in the 13.5 nm particle, we extracted a single ring out of the final reconstruction of the large complex and calculated the correlation coefficient between the ring density and itself rotated around the putative symmetry axis at 30 Å resolution [18]. Remarkably, one plateau was observed every fifty degrees (Fig. 8A). In addition, we calculated the rotational power spectrum [21], which clearly indicated the 7-fold symmetrical character of the 7.5 nm diameter particle (Fig. 8B).

Based on all these results, we propose that an individual $DdrA_{(1-160)}$ ring is a heptamer and attribute the seven density bulges located around the pronounced central cavity of 35 Å in diameter to seven $DdrA_{(1-160)}$ monomers (Fig. 7).

Finally, to determine the relative arrangement of the seven subunits, seven copies of the N-terminal domain of the Rad52 monomer (residues ranged from 25 to 178) were fitted into the electron microscopy map of the extracted single ring [18]. Without any imposed symmetry, the monomers adopted a nearly symmetrical distribution around the ring axis, with a correlation coefficient and a R-factor between 400 and 25 Å resolution of 94.5% and 37.1%, respectively. In comparison, fitting the subunits turned upside down gives a correlation coefficient and a R-factor of 92.8% and 41.4%, respectively. This resulting model of the $DdrA_{(1-160)}$ heptamer was then placed into the electron microscopy map of the 3-ring complex (Fig. 7). In this model, the accessible surface buried between two monomers is 2300 $Å^2$ and 500 $Å^2$ between two heptamers in the 3-ring assembly.

4. Discussion

The *Deinococci* bacteria have the remarkable capacity to tolerate and repair massive DNA damages. Among their original genes with unknown function, the *ddrA* gene was clearly identified as related to the radiotolerance and the genome restitution [3,5]. We provide a three-dimensional reconstruction of the *D. deserti* $DdrA_{(1-160)}$ showing that the truncated DdrA has a complex architecture based on a 7.5 nm diameter ring composed of seven monomers (Fig. 7). This basic structural motif can also self-associate to form larger molecular weight structures as the 3-ring assembly presented here. The nearly symmetrical distribution of the seven subunits around the rotational axis of each ring (Figs. 7 and 8) suggests that an individual ring of $DdrA_{(1-160)}$ should have a perfect seven-fold symmetry. This symmetry would be slightly disturbed by the contacts between the adjacent rings within the 3-ring assemblies.

Based on the DNA binding properties and the radiotolerance phenotype of $DdrA_{(1-160)}$, we propose that the wild type DdrA structure would exhibit two functional regions: a basic N-terminal region necessary and sufficient to bind specifically the single-stranded DNAs, and the last C-terminal residues essential to the radiotolerance

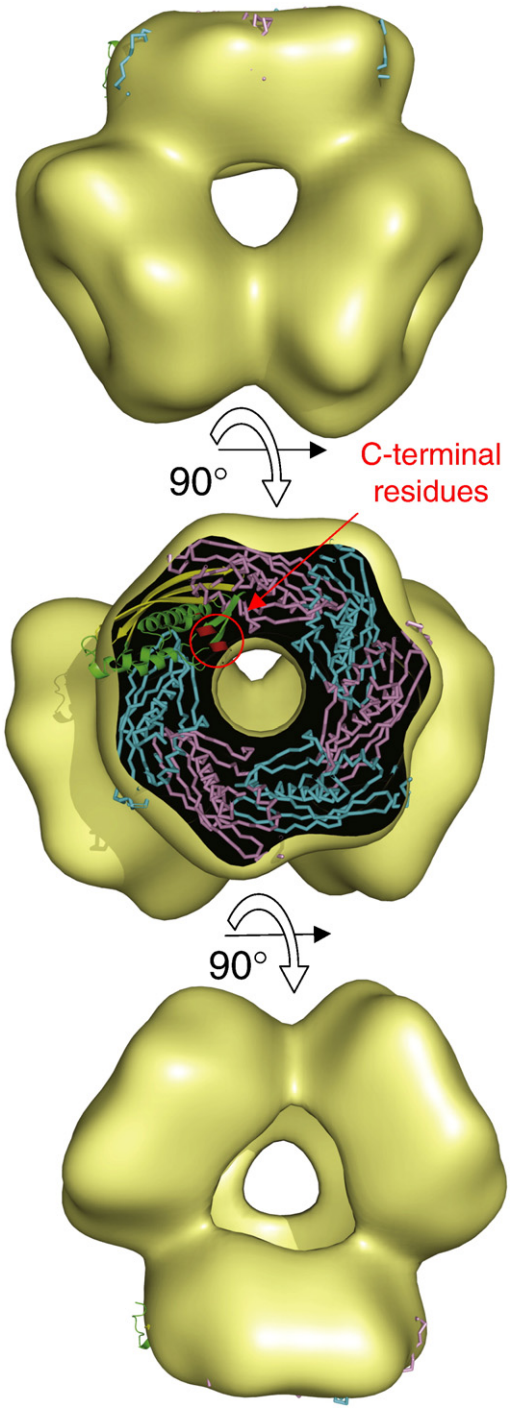

Fig. 7. Three-dimensional reconstruction of $DdrA_{(1-160)}$ 3-ring particle. The 3-fold symmetry clearly appears in the top and bottom views. The central view shows the pseudo seven-fold axis perpendicular to the image plan with a fit of seven N-terminal domains of Rad52 monomer (PDB ID: 1KN0, only residues 25 to 178 were considered) into the electron microscopy reconstruction. To distinguish the different monomers, they were colored in cyan or pink. The seventh monomer is represented with b-strand and helical structures colored in yellow and green, respectively. The last C-terminal residues are shown in red. This figure was generated by Pymol (pymol.sourceforge.net).

phenotype but not critical for the binding of DNA. We suggest that the C-terminal domain might be involved in the interaction with other cellular components required for an efficient DNA double strand break repair. In particular, DdrA could be important not only for preventing extensive genome degradation after DNA damage and for ensuring long-lived recombinational substrates and recycling of RecA protein [22], but also for the recruitment of proteins involved in double-strand break repair. The identification of these partners and the detection of the different complexes that DdrA may form *in vivo*, would greatly help to understand the precise function of DdrA in the DNA repair processes.

Our present results support a pronounced structural and functional similarity between the bacterial DdrA and eukaryotic Rad52 proteins [4]. Even if the sequence identity between Rad52 and DdrA is relatively weak, the predicted secondary structure organization pinpointed that *D. deserti* DdrA fold would resemble the one of the truncated $Rad52_{(1-209)}$ monomer [4,23]. As we propose for the full-length DdrA, Rad52 also consists in two structural domains [24]: the N-terminal domain (1–209) required for the single-stranded DNA annealing that oligomerizes as a ring structure, and the C-terminal domain (210–419) supposed to activate the Rad51 enzyme, the functional analogue of the bacterial RecA recombinase [25]. In addition, like $DdrA_{(1-160)}$, the truncated $Rad52_{(1-209)}$, binds single-stranded DNA ends as the complete protein but is not functional [23,24]. Previous electron microscopy studies showed that the full-length Rad52 structure was a heptameric ring [26] like $DdrA_{(1-160)}$. However, in contrast to the wild-type protein, $Rad52_{(25-209)}$ crystallized as an undecameric ring [23,24] and we cannot exclude that this structural resemblance between the full-length Rad52 and $DdrA_{(1-160)}$ may be coincidental and that the removal of the C-terminal residues might influence the oligomerization state of DdrA as the truncation of the whole C-terminal domain of Rad52 did [27]. Even if no 3D structure of the full-length DdrA is available yet, we speculate that these structural similarities between $DdrA_{(1-160)}$ and Rad52 could translate a common biological function. Since no data that could indicate a potential activity in strand annealing has been reported for DdrA, the functional parallel between DdrA and Rad52 may be limited to the binding of single-stranded DNA ends during the DNA repair.

The DNA binding affinity of DdrA is also very intriguing. The structural resemblance between both proteins allowed a good docking of the Rad52 N-terminal domain [23,24] (residue range: 25 to 178) into $DdrA_{(1-160)}$ electron microscopy reconstruction (Fig. 7). In this hypothetical model of DdrA, the anti-parallel β-sheets from seven monomers would line up the central cavity of the heptamer. Because β-secondary structures are present in many single-stranded DNA binding proteins (like the OB-fold [28]), we suggest that the DNA molecules would wrap this β-strand structure. This binding site resulting from the oligomerization could accommodate long oligonucleotides.

Besides, the high proportion of basic residues in the DdrA sequences (Fig. 3) suggests that DNA recognition would be driven by electrostatic interactions between the phosphate backbone of the DNA molecule and the positively charged residues of the protein as it was shown for numerous other DNA binding proteins. However, electrostatic contacts are certainly not the only driving strength. DdrA does not bind double-stranded DNA [5] (Fig. 6) and this can be explained by the difference of plasticity between the single-stranded DNA and the canonical double helix [29]. The complex architecture of DdrA (shape and high oligomeric state) should induce some constraints on the DNA molecules that can only be achieved by the most flexible molecules, *i.e*, the single-stranded oligonucleotides. In addition, in DdrA, the polarity of the DNA is a major factor as 3′-single-stranded ends are significantly better recognized than 5′-single-stranded ends [5] (Fig. 6). As demonstrated by *in vitro* DNA binding assays on purified oligonucleotides and DdrA, this substrate discrimination does not require other cellular components. In the absence of a high resolution structure of the DdrA–DNA complex that will reveal the detailed DNA binding mode of DdrA, we suggest the prevalence of specific polar and hydrophobic contacts between the protein and the nucleotide sugar and base moieties that will guide the DNA binding and favor one type of single-stranded DNA ends. Those interactions would contribute highly to the ligand discrimination.

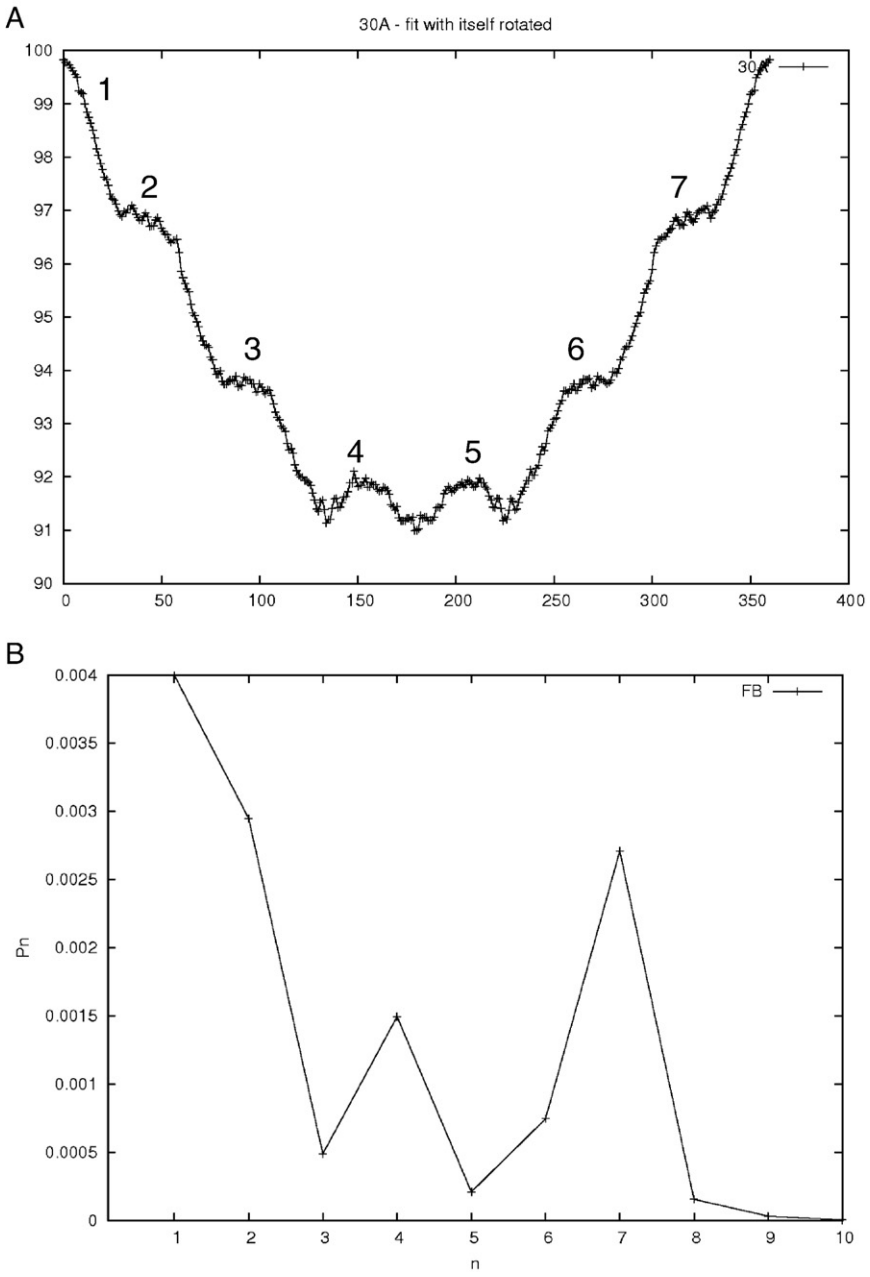

Fig. 8. Confirmation of the C7 symmetry: A) Correlation coefficient calculated between the ring density and itself rotated from 0 to 360° around the putative symmetry axis. The correlation coefficients were calculated by the UROX program [18]. One plateau is observed every fifty degrees. B) Rotational power spectrum (Pn) versus symmetry order (n) calculated as described in [21]. The seven-fold symmetry is clearly indicated. An additional pseudo two-fold symmetry is detected in the rotational spectrum in agreement with the symmetrical appearance around 180°.

Our electron microscopy study describes two types of $DdrA_{(1-160)}$ multimers. We cannot predict if both structures co-exist *in vivo*. However, the estimated value of the buried accessible surface between the monomers in the hypothetical $DdrA_{(1-160)}$ model translates a strong internal cohesion of the heptamer in contrast to the interaction between each ring, which is relatively weak. This could explain presence of a mixture of single rings and 3-ring assemblies on the electron microscopy grid.

The basket shaped model we described, would not be the most stable state but we cannot exclude that the stability of the three-ring assembly may be influenced by the DNA presence. Early preliminary gel filtration analysis suggested that *D. radiodurans* DdrA would be composed of 8 to 10 subunits [4], which compares to the single heptameric ring particle of *D. deserti* $DdrA_{(1-160)}$ that exhibits a strong stability. All these observations support the hypothesis that the heptameric ring is a biologically relevant entity. Our hypothetical model of DdrA also suggests that the C-terminal residues removed in the truncated form $DdrA_{(1-160)}$, would not be involved in the contacts between the heptamers (Fig. 7) and thus, we suppose that similar large multimeric assemblies could be obtained with the full-length protein as well. In the cell, the large assemblies could correspond to a transient state occurring during the DNA repair to put together the repair machinery including several DNA single strands and other unknown cellular partners. A complex pattern of self-association also described for the wild type and truncated forms of Rad52, was suggested important to promote DNA end-joining [27]. Such a large complex organization and conformational flexibility would optimize the interactions between these different molecular elements. In that context, the dynamics and the supra-structure of DdrA would play an important functional role and could favor a rapid and efficient DNA repair.

Acknowledgements

The authors would like to thank the CEA, CNRS and EDF for their financial support. AVŽ is a recipient of a research grant for foreigner attributed by the "Commissariat à l'Energie Atomique". We are also very grateful to P. Amara for her critical reading. We would like to thank D. Lascoux for the mass spectroscopy analysis and G. Schoehn for the initial observations performed on the microscopy platform at the PSB (Grenoble). We thank the "Institut Curie" for the use of the ^{137}Cs irradiation system and V. Favaudon for his assistance.

References

[1] K. Zahradka, D. Slade, A. Bailone, S. Sommer, D. Averbeck, M. Petranovic, A.B. Lindner, M. Radman, Repair of shattered chromosomes in *Deinococcus radiodurans*: a natural contig assembly, Nature 443 (2006) 569–573.
[2] Y. Liu, J. Zhou, M.V. Omelchenko, A.S. Beliaev, A. Venkateswaran, J. Stair, L. Wu, D.K. Thompson, D. Xu, I.B. Rogozin, E.K. Gaidamakova, M. Zhai, K.S. Makarova, E.V. Koonin, M.J. Daly, Transcriptome dynamics of *Deinococcus radiodurans* recovering from ionizing radiation, Proc. Natl. Amer. Soc. 100 (2003) 4191–4196.
[3] M. Tanaka, A.M. Earl, H.A. Howell, M.J. Park, J.A. Eisen, S.N. Peterson, J.R. Battista, Analysis of *Deinococcus radiodurans*'s transcriptional response to ionizing radiation and desiccation reveals novel proteins that contribute to extreme radioresistance, Genetics 168 (2004) 21–33.
[4] L.M. Iyer, E.V. Koonin, L. Aravind, Classification and evolutionary history of the single-strand annealing proteins, RecT, Redbeta, ERF and Rad52, B.M.C. Genomics 3 (2002) 8.
[5] D.R. Harris, M. Tanaka, S.V. Saveliev, E. Jolivet, A.M. Earl, M.M. Cox, J.R. Battista, Preserving genome integrity: the DdrA protein of *Deinococcus radiodurans* R1, PLoS Biol. 2 (2004) e304.
[6] H. Brim, A. Venkateswaran, H.M. Kostandarithes, J.K. Fredrickson, M.J. Daly, Engineering *Deinococcus geothermalis* for bioremediation of high-temperature radioactive waste environments, Appl. Environ. Microbiol. 69 (2003) 4575–4582.
[7] A. de Groot, V. Chapon, P. Servant, R. Christen, M. Fischer-Le Saux, S. Sommer, T. Heulin, *Deinococcus deserti* sp. nov. a gamma-radiation-tolerant bacterium isolated from the Sahara Desert. Int. J. Syst. Evol. Microbiol. 55 (2005) 2441–2446.
[8] K.S. Makarova, M.V. Omelchenko, E.K. Gaidamakova, M.J. Daly, *Deinococcus geothermalis*: the pool of extreme radiation resistance genes shrinks, Plos ONE 2 (2007) e955.
[9] R. Meima, H.M. Rothfuss, L. Gewin, M.E. Lidstrom, Promoter cloning in the radioresistant bacterium *Deinococcus radiodurans*, J. Bacteriol. 183 (2001) 3169–3175.
[10] C. Bonacossa de Almeida, G. Coste, S. Sommer, A. Bailone, Quantification of RecA protein in *Deinococcus radiodurans* reveals involvement of RecA, but not LexA, in its regulation, Mol. Genet. Genomics 268 (2002) 28–41.
[11] S. Mennecier, G. Coste, P. Servant, A. Bailone, S. Sommer, Mismatch repair ensures fidelity of replication and recombination in the radioresistant organism *Deinococcus radiodurans*, Mol. Genet. Genomics 272 (2004) 460–469.
[12] K. Houben, D. Marion, N. Tarbouriech, R.W.H. Ruigrok, L. Blanchard, Interaction of the C-terminal domains of Sendai virus N and P proteins: comparison of polymerase-nucleocapsid interactions within the paramyxovirus family, J. Virol. 81 (2007) 6807–6816.
[13] J.A. Cuff, M.E. Clamp, A.S. Siddiqui, M. Finlay, G.J. Barton, Jpred: a consensus secondary structure prediction server, Bioinformatics 14 (1998) 892–893.
[14] S. Miyazaki, Y. Kuroda, S. Yokoyama, Characterization and prediction of linker sequences of multi-domain proteins by a neural network, J. Struct. Funct. Genomics 2 (2002) 37–51.
[15] E. Gasteiger, C. Hoogland, A. Gattiker, S. Duvaud, S.M.R. Wilkins, R.D. Appel, A. Bairoch, Protein identification and analysis tools on the ExPASy server, in: J.M. Walker (Ed.), The Proteomics Protocols Handbook, Humana Press, 2005, pp. 571–607.
[16] M. Van Heel, G. Harauz, E.V. Orlova, R. Schmidt, M. Schatz, A new generation of the IMAGIC image processing system, J. Struct. Biol. 116 (1996) 17–24.
[17] S.J. Ludtke, P.R. Baldwin, W. Chiu, EMAN: semiautomated software for high-resolution single-particle reconstructions, J. Struct. Biol. 128 (1999) 82–97.
[18] J. Navaza, J. Lepault, F.A. Rey, C. Alvarez-Rua, J. Borge, On the fitting of model electron densities into EM reconstructions: a reciprocal-space formulation, Acta Crystallogr. D 58 (2002) 1820–1825.
[19] Collaborative Computational Project, Number 4, the CCP4 Suite: programs for protein crystallography, Acta Crystallogr. D 50 (1994) 760–763.
[20] I.L. Hofacker, Vienna RNA secondary structure server, Nucleic Acids Res. 31 (2003) 3429–3431.
[21] R.A. Crowther, L.A. Amos, Harmonic analysis of electron microscope images with rotational symmetry, J. Mol. Biol. 60 (1971) 123–130.
[22] E. Jolivet, F. Lecointe, G. Coste, K. Satoh, I. Narumi, A. Bailone, S. Sommer, Limited concentration of RecA delays DNA double-strand break repair in *Deinococcus radiodurans* R1, Mol. Microbiol. 59 (2006) 338–349.
[23] W. Kagawa, H. Kurumizaka, R. Ishitani, S. Fukai, O. Nureki, T. Shibata, S. Yokoyama, Crystal structure of the homologous-pairing domain from the human Rad52 recombinase in the undecameric form, Mol. Cell 10 (2002) 359–371.
[24] M. Singleton, L. Wentzell, Y. Liu, S. West, D. Wigley, Structure of the single-strand annealing domain of human Rad52 protein, Proc. Natl. Amer. Soc. 99 (2002) 13492–13497.
[25] G.T. Milne, D.T. Weaver, Dominant negative alleles of RAD52 reveal a DNA repair/recombination complex including Rad51 and Rad52, Genes Dev. 7 (1993) 33–49.
[26] A.Z. Stasiak, E. Larquet, A. Stasiak, S. MĬller, A. Engel, E. Van Dyck, S.C. West, E.H. Egelman, The human Rad52 protein exists as a heptameric ring, Curr. Biol. 10 (2000) 337–340.
[27] W. Ranatunga, D. Jackson, J.A. Lloyd, A.L. Forget, K.L. Knight, G.E.O. Borgstahl, Human RAD52 exhibits two modes of self-association, J. Biol. Chem. 276 (2001) 15876–15880.
[28] Y. Shamoo, Single-stranded DNA binding proteins, Macmillian publishers Ltd. *Encyclopedia of life sciences*, Nature publishing group, 2002, pp. 1–7.
[29] G.M. Blackburn, M.J. Gait, Interaction of proteins with nucleic acids, Nucleic acids in chemistry and biology, Oxford University press, 1996, pp. 376–441.
[30] P. Gouet, E. Courcelle, F. Metoz, ESPript: analysis of multiple sequence alignments in postscript, Bioinformatics 15 (1999) 305–308.
[31] A.W. Anderson, H.C. Nordon, R.F. Cain, G. Parrish, G. Duggan, Studies on a radioresistant *micrococcus*. Isolation, morphology, cultural characteristics, and resistance to gamma radiation, Food Technol. 10 (1956) 575–578.
[32] F. Lecointe, G. Coste, S. Sommer, A. Bailone, Vectors for regulated gene expression in the radioresistant bacterium *Deinococcus radiodurans*, Gene 336 (2004) 25–35.